ASTM D5946
ASTM D7334
ASTM D7490
ISO 27448

optical contact angle measurements and drop contour analysis to determine surface energy as well as interfacial and surface tension

force tensiometry, dynamic contact angle measurements, and force of adhesion evaluation

ASTM D1331
ASTM D1417
ISO 1409

ISO/TR 13097

optical turbidity, stability and aging analysis of multi-phase dispersions

zeta potential measurements of fibres, powders, and plate-shaped solids

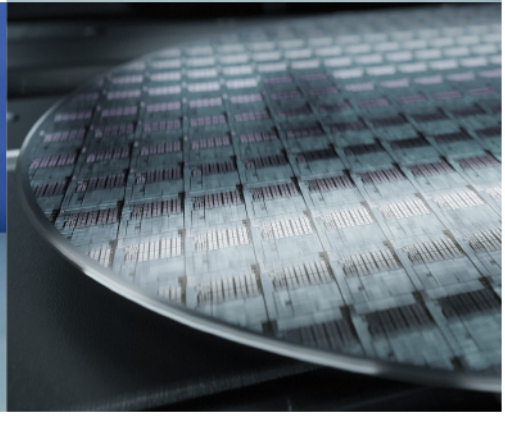

High-end, versatile laboratory measurement device portfolio for a comprehensive analysis of surfaces and interfaces

Learn more >

dataphysics
Understanding Interfaces

DataPhysics Instruments GmbH
Raiffeisenstraße 34 • 70794 Filderstadt, Germany
phone +49 (0)711 770556-0 • fax +49 (0)711 770556-99
sales@dataphysics-instruments.com
www.dataphysics-instruments.com

ADVANCED FUNCTIONAL MATERIALS
www.afm-journal.de

Check for updates

Laser-Induced, Green and Biocompatible Paper-Based Devices for Circular Electronics

Giuseppe Cantarella, Mallikarjun Madagalam, Ignacio Merino, Christian Ebner, Manuela Ciocca, Andrea Polo, Pietro Ibba, Paolo Bettotti, Ahmad Mukhtar, Bajramshahe Shkodra, AKM Sarwar Inam, Alexander J. Johnson, Arash Pouryazdan, Matteo Paganini, Raphael Tiziani, Tanja Mimmo, Stefano Cesco, Niko Münzenrieder, Luisa Petti, Nitzan Cohen, and Paolo Lugli*

The growing usage and consumption of electronics-integrated items into the daily routine has raised concerns on the disposal and proper recycling of these components. Here, a fully sustainable and green technology for the fabrication of different electronics on fruit-waste derived paper substrate, is reported. The process relies on the carbonization of the topmost surface of different cellulose-based substrates, derived from apple-, kiwi-, and grape-based processes, by a CO_2 laser. By optimizing the lasing parameters, electronic devices, such as capacitors, biosensors, and electrodes for food monitoring as well as heart and respiration activity analysis, are realized. Biocompatibility tests on fruit-based cellulose reveal no shortcoming for on-skin applications. The employment of such natural and plastic-free substrate allows twofold strategies for electronics recycling. As a first approach, device dissolution is achieved at room temperature within 40 days, revealing transient behavior in natural solution and leaving no harmful residuals. Alternatively, the cellulose-based electronics is reintroduced in nature, as possible support for plant seeding and growth or even soil amendment. These results demonstrate the realization of green, low-cost and circular electronics, with possible applications in smart agriculture and the Internet-of-Thing, with no waste creation and zero or even positive impact on the ecosystem.

1. Introduction

As presented by the 2030 Agenda for Sustainable Development adopted by the United Nations,[1] the general awareness on the ecological, financial, social, and material sustainability around every aspect of our society is continuously increasing. Urgent actions are required by all countries to protect our planet, preserve natural resources and ensure sustainable consumptions and production patterns. Considering the unbridled diffusion of Internet-of-Things (IoT), this green and sustainable revolution also includes the electronic devices.[2] Indeed, growing attention is being devoted to fabrication protocols, devices and systems, employing reusable and recyclable materials, limiting the use of Earth-rare elements, and reducing waste after electronics dismissing (e-waste).[3] Despite recent progress, significant actions are still required to recycle materials effectively.[4] To support

G. Cantarella
Department of Physics, Informatics and Mathematics
University of Modena and Reggio Emilia
41125 Modena, Italy
E-mail: giuseppe.cantarella@unimore.it

M. Madagalam
Department of Applied Science and Technology
Politecnico di Torino
10129 Torino, Italy

The ORCID identification number(s) for the author(s) of this article can be found under https://doi.org/10.1002/adfm.202210422.

© 2023 The Authors. Advanced Functional Materials published by Wiley-VCH GmbH. This is an open access article under the terms of the Creative Commons Attribution License, which permits use, distribution and reproduction in any medium, provided the original work is properly cited.

DOI: 10.1002/adfm.202210422

I. Merino, N. Cohen
Faculty of Design and Art
Free University of Bozen-Bolzano
39100 Bolzano, Italy

C. Ebner, M. Ciocca, A. Polo, P. Ibba, A. Mukhtar, B. Shkodra, A. S. Inam, R. Tiziani, T. Mimmo, S. Cesco, N. Münzenrieder, L. Petti, P. Lugli
Faculty of Science and Technology
Free University of Bozen-Bolzano
39100 Bolzano, Italy

P. Bettotti
Nanoscience Laboratory, Department of Physics
University of Trento
38123 Trento, Italy

A. J. Johnson, A. Pouryazdan
Sensor Technology Research Centre
University of Sussex. Falmer
Brighton BN1 9QT, UK

M. Paganini
Environmental Physiology Lab, Department of Biomedical Sciences
University of Padova
35121 Padova, Italy

16163028, 0, Downloaded from https://onlinelibrary.wiley.com/doi/10.1002/adfm.202210422 by University Of Padova Center Di, Wiley Online Library on [21/02/2023]. See the Terms and Conditions (https://onlinelibrary.wiley.com/terms-and-conditions) on Wiley Online Library for rules of use; OA articles are governed by the applicable Creative Commons License

16163028, 0, Downloaded from https://onlinelibrary.wiley.com/doi/10.1002/adfm.202210422 by University Of Padova Center Di, Wiley Online Library on [21/02/2023]. See the Terms and Conditions (https://onlinelibrary.wiley.com/terms-and-conditions) on Wiley Online Library for rules of use; OA articles are governed by the applicable Creative Commons License

this green transition, different approaches are investigated. First, alternative sustainable materials, which have to fulfill specific requirements, including programmable dissolution[5,6] and biodegradability,[7,8] need to be deployed. In this perspective, hydrogels,[9,10] soft polymers,[11] and plant-derived natural compounds[12] have showed stable performance as conductors, insulators and semiconductors.[13] Among these, the use of paper or cellulose-based materials has been widely explored as substrate material[14] for flexible electronics. Although reliable recycling processes allow infinite and sustainable reuse of cellulose, the materials employed in the device stack (i.e., toxicants, pollutants, rare-Earth elements) are still limiting factors, to achieve a green transition.[15] In parallel to theuse of alternative materials, a reliable and energy-conscious technology for electronics fabrication requires other special features, such as large-area processability, limited power consumption, and low fabrication cost. Especially for this latter requirement, it is crucial to investigate several aspects, including the materials supply chain, the investment and running costs for equipment, as well as the employment of affordable raw materials in the electronics stack. Although widely employed for micro- and nanoelectronics applications, vacuum-based deposition methods (i.e., evaporation, sputtering) are indeed not cost-effective. In order to guarantee large-area processability with limited cost, printing technology (e.g., screen printing, roll-to-roll, ink-jet, etc.) represents an important step forward for commercialization of electronics.[16–18] Among all, laser-induced carbonization is especially interesting and it consists in the employment of laser scriber setups, often used for wood and plastic engraving, on carbon-rich substrates, such as polyimide (PI), Kevlar, poly (ether imide) (PEI), wood, natural cork, coal, and paper.[19–27] The possibility of large-scale manufacturing (up to m^2 scale) in combination with quick reproduction of different patterns by software manipulation has dramatically increased the employment of this technique for devices fabrication. This has allowed the realization of a broad range of electronics, such as sensors,[28–30] solar cells,[31] electro-actuators,[32,33] generators, antennas,[34] and supercapacitors.[35] Although paper substrates have been combined with laser-induced carbonization,[36–40] a limited device range has been presented so far and the potential of this natural material (i.e., recyclability, natural dissolution, no harmful residuals) is not yet fully exploited.

Here, we report a fully sustainable, green, and circular electronics platform, using paper substrates, obtained from processing fruit wastes, and laser writing. These substrate materials are made by processing by-product from apple, grape, and kiwi, to drastically replace virgin tree pulp. First, the optimization of the laser writing parameters is carried out on different papers (apple-, kiwi-, and grape-based papers), to achieve minimum sheet resistance and to optimize quality of the carbonized layer. Then, the large area capability of the lasing process as well as the insulating nature of the cellulose-based substrate is exploited to realize a broad range of electronics devices. Initially, capacitors and biosensors are demonstrated. Next, to highlight the suitability and performances of these devices, several example applications are investigated. To prove device functionality for on-skin applications, disposable, and low-cost electrodes, with reliable and stable performance for heart-activity and respiratory monitoring, are realized. Skin-electrodes biocompatibility is confirmed on human dermal fibroblasts. Additionally, device functionality is studied for impedance spectroscopy on fruits (apple and banana), to monitor the maturity stage and its application for on field and smart agriculture. To evaluate how this paper-based electronics platform can contribute towards circular and fully sustainable technology, two recycling methods are also analyzed. First, dissolution tests in nontoxic solutions (i.e., lemon juice) are conducted, showing device functionality for temporal usage (40 days), before degradation while avoiding e-waste creation. Second, germination tests are performed on our laser-induced electronics, proving seed growth within 72 h, supporting plant growth. A schematic of the circular flow is depicted in **Figure 1**.

2. Results

2.1. Parameters Optimization and Material Analysis

An optical picture of the employed paper is shown in Figure 1. These commercially available substrate materials (Favini, Crush Paper) are achieved by using process by-product from apple, grape, and kiwi, to drastically replace virgin tree pulp. This approach allows a significant step ahead toward a fully sustainable technology, thanks to a reduction of natural resources employed (i.e., cellulose), as well as the usage of food waste products. In order to minimize the sheet resistance out of these papers, it is crucial to optimize the laser writing properties, which includes laser power (0 W ≤ power ≤ 60 W), laser speed (0 mm s^{-1} ≤ speed ≤ 4200 mm s^{-1}) and defocus. Test structures (rectangular stripes of 3 mm × 30 mm) are first used while varying these three parameters and using a single laser pass, even if no electrical conductivity is measured. Indeed, the resulting layers are either barely carbonized or highly damaged (see Figure S1, Supporting Information). As a first step to improve the fabrication method, a flame retardant solution is applied on the paper, to minimize the risk of fiber damage due to laser irradiation.[38] Initially, the solution is manually sprayed on both sides of the papers from a distance of 10 cm, and the sheet resistance is measured. Although a consistent improvement is denoted (here, single lasing sweep is performed), with minimum sheet resistance of 709 Ω Υ^{-1} ± 99 Ω Υ^{-1}, 648 Ω Υ^{-1} ± 112 Ω Υ^{-1}, and 393 Ω Υ^{-1} ± 126 Ω Υ^{-1}, for grape-, kiwi-, and apple-based papers, respectively, the resistance trend shows high variability between two consecutive points of the plot (see Figure S2, Supporting Information), and therefore, low reliability of the lasing process. To reduce the variability from sample to sample, and increase the material uniformity, all three papers are immerged in the flame retardant (FR) solution prior lasing, monitoring the results as function of the immersion time. Test structures are fabricated and evaluated on each of the three substrates, by varying laser power (3 or 4.2 W), laser speed (from 210 to 1050 mm s^{-1}, with 42 mm s^{-1} step), immersion time (10, 90 min, 2.5, 4, 5.5, 8 h), while keeping constant defocus (5 mm; see Figures S3–S5, Supporting Information). For parameters out of the selected ranges (i.e., immersion time > 8 h, laser speed < 210 mm s^{-1}, laser speed > 1050 mm s^{-1}), no significant reduction of the sheet resistance is observed. Since electrical conductivity of all paper substrates are comparable,

© 2023 The Authors. Advanced Functional Materials published by Wiley-VCH GmbH

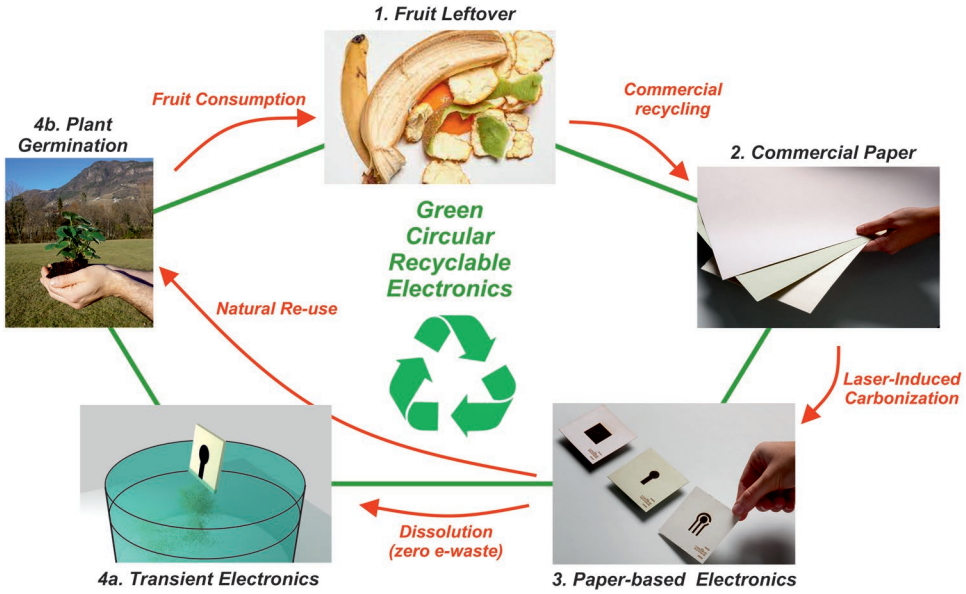

Figure 1. Sketch of the circular technology based on laser-induced electronics. A paper substrate derived from fruit waste is utilized. The employment of large-area and low-cost fabrication method allows the realization of a broad range of electronics. By the end of their life cycle, devices can dissolve in natural solutions, or can be used for plant germination and growth. In this way, no electronic-waste (e-waste) is generated and any negative impact on the ecosystem is avoided.

we choose the apple one as it require the shorter immersion time to achieve the optimal conductivity (2.5 h for both apple-based and kiwi, 5.5 h for grape-based) and it provides the best reproducibility (i.e., smaller standard deviation, ±25 Ω Υ^{-1} for apple-based, ±71 Ω Υ^{-1} for grape-based and ±95 Ω Υ^{-1} for kiwi-based) (see **Figure 2**a). This optimized sheet resistance of 366 Ω Υ^{-1} ± 25 Ω Υ^{-1} is achieved with laser speed, power, defocus and immersion time equal to 378 mm s^{-1}, 3 W, 5 mm, and 2.5 h, respectively (see Figure S5, Supporting Information).

To estimate the engraving effect of these optimized parameters, thickness evaluation of the carbonized part is performed. Optical microscope pictures and profilometer analysis reveal an averaged depth of 37 µm (overall paper thickness before lasing equal to 295 µm; see Figure S6, Supporting Information). This thickness is directly affected by all parameters, and it can be modified, according to the specific application. Raman spectroscopy is utilized to properly evaluate the quality of the carbonized layers. The D and G peaks, at 1350 and 1580 cm^{-1},

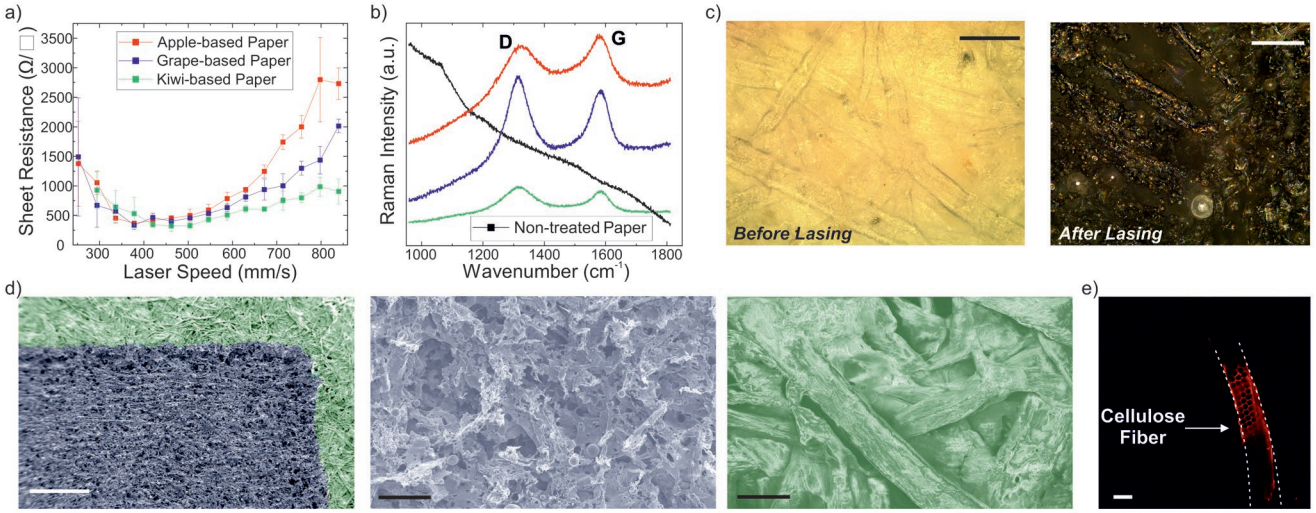

Figure 2. Material analysis and characterization. The optimized lasing parameters are evaluated through electrical, chemical, and optical properties. a) Sheet resistance as function of laser speed and b) Raman spectroscopy for the three paper types. c) Surface morphology analysis of the paper surface reveals the effect on the lasing process before and after the carbonization (Scale bar: 50 µm). d) 26° tilted and colored SEM image of a carbonized layout (Scale bar: 500 µm), with zoom on both carbonized layer (Scale bar: 50 µm) and cellulose fibers (Scale bar: 20 µm). e) Confocal fluorescence image of a cellulose fiber, with honeycomb structures, confirming the presence of fruit residuals (Scale bar: 30 µm).

© 2023 The Authors. Advanced Functional Materials published by Wiley-VCH GmbH

16163028, 0, Downloaded from https://onlinelibrary.wiley.com/doi/10.1002/adfm.202210422 by University Of Padova Center Di, Wiley Online Library on [21/02/2023]. See the Terms and Conditions (https://onlinelibrary.wiley.com/terms-and-conditions) on Wiley Online Library for rules of use; OA articles are governed by the applicable Creative Commons License

16163028, 0, Downloaded from https://onlinelibrary.wiley.com/doi/10.1002/adfm.202210422 by University Of Padova Center Di, Wiley Online Library on [21/02/2023]. See the Terms and Conditions (https://onlinelibrary.wiley.com/terms-and-conditions) on Wiley Online Library for rules of use; OA articles are governed by the applicable Creative Commons License

respectively, and the absence of 2D peak (≈2700 cm^{-1}) proves the amorphous nature of the carbonized layer on all the cellulose substrates under investigation (see Figure 2b).[19,41] Further optimization of the writing process (i.e., multiple lasing pass,[19] inert atmosphere,[42] etc..) can tune the material quality (defect density, strain, doping concentration) and the material type (graphite, graphene). At the microscale, the carbonization process is evident while analyzing the surface morphology of both the paper and of the carbonized layer (see Figure 2c,d). Before carbonization, a clear network of cellulose fibers, with lateral size ranging from 5 to 30 µm, is visible (see Figure 2c). At this stage, confocal fluorescence microscope imaging is used to analyze the virgin paper surface (see Figure 2e). Using red fluorochromes (see Experimental section – Cell culture, adhesion, viability, and proliferation), honeycomb-like structures are visible on the cellulose fibers, showing tissue structures comparable to fruit samples.[43,44] After lasing, the surface is rougher and the carbonized fibers are less visible (see Figure 2c–d). To further investigate the full potential of the lasing process, resolution studies are performed to analyze the minimum spot size achievable with our system. Circles with variable diameter, ranging from 1 to 300 µm, are designed and reproduced on different papers (apple, as main substrate, and kiwi, to support the results) using an optimized defocus (equal to 5 mm) and no focus (0 mm; see Table. S1, Supporting Information). In optimal condition (defocus equal to 5 mm and using apple substrate), a minimum resolution of 640 µm is achieved. Comparing circles lased with the same focus condition (5 mm or 0 mm), low variability (<±54 µm) is denoted between the employed substrates, proving the quality of the lasing process on any carrier (see Table S1, Supporting Information). Patterns, reproduced with optimized defocus (=5 mm), show contours with higher definition, whereas structures fabricated without defocus exhibit higher roughness and deeper engraving of the paper (see Figure S7, Supporting Information).

2.2. Devices and Applications

The optimization of the laser process on fruit-based paper substrate allows the low-cost and large-area fabrication of a broad range of flexible and paper-based electronics. To evaluate the capabilities of this technology, electronic devices are fabricated and electrically-characterized on apple-based substrate (see Experimental section – Substrate Preparation and Induced Carbonization) due to the shorter immersion time in FR solution and the best reproducibility. Taking advantage of the insulating property of the cellulose, parallel plate capacitors are realized. Here, devices with different plate areas, ranging from 1.5 to 45 mm^2 are characterized (see **Figure 3**a,b), reporting tunable capacitances from 0.5 to 16 pF, loss tangent from 0.46 to 0.90 and a dielectric permittivity of 2.9 at 5 MHz (see Figure 3c) (see Experimental Section – Electrical Characterization section).[45–47] In addition, frequency response up to 100 kHz is reported for magnitude, phase, and loss tangent (see Figure S8, Supporting Information), allowing appropriate bandwidth for different applications, e.g., wearables and disposable IoT. The combination of this technology with methods for low-cost deposition of semiconductors, such as spray-coating or spin coating, can allow the realization of large-area and flexible active electronics (e.g., transistors and circuits), avoiding vacuum processing (i.e., evaporation, magnetron sputtering), and structuring technique (i.e., shadow masking, photolithography).[14,48]

For diagnostic, technological trends are moving toward new systems with rapid response and low to moderate cost, while leading to precise and accurate outputs. In this respect, biosensors are widely known devices for detection of chemical and biological analytes, which have found broad application in environmental monitoring,[49] food quality analysis,[50,51] and medicine.[52,53] Although several examples of laser induced biosensors have been reported,[30,54–56] the employment of PI as carrier substrate is still a limiting factor to achieve a fully

sustainable, disposable, and environmentally friendly devices. As proof of concept, a three-electrodes design, consisting of carbonized working, counter and reference electrodes, is implemented on cellulose substrate (see Figure 3d). For performance comparison, cyclic voltammetry (CV) of our device and a commercial carbon-based one, using 5 mM $[Fe(CN)_6]^{3-/4-}$ in 0.1 M KCl as electrolyte solution, is used as shown in Figure 3d. After three measurements, the two devices show low variability between measurements (maximum variation equal to 0.27 mA), maximum oxidation current peaks of 226 µA on cellulose substrate and 239 µA for the commercial one, and a potential difference between the oxidation and reduction peaks ΔE_p of 0.14 and 0.22 V. The shift in the oxidation/reduction peaks is also correlated to the nature of the employed carbon materials: amorphous and laser-induced for the paper-based device; screen printed, for the commercial sensor. This gives rise to performance variations, which strictly depend on the material intrinsic properties (i.e., molecular structure, dimensions).[57,58] Although graphene is prominent for electron transfer,[59,60] the performances of our carbonized biosensor-like electrodes on apple-based paper are similar to other devices, fabricated with laser-induced graphene and on PI substrate.[28,54,56] To expand this device functionality toward a real market scenario and fulfill specific applications (i.e., high selectivity, detection of low concentration, etc.), additional studies and treatments[61] will be required to demonstrate selectivity to specific analytes, moving toward paper-based, sustainable, and disposable point-of-care.[62]

Similarly to biosensing, the field of health monitoring is continuously demanding new electronic systems, enabling efficient collection of physiological indicators, unobtrusive, and lightweight, to support facile on-skin usage. Although several laser-induced based sensors have been demonstrated[63] on plastic foils (i.e., PI), biocompatible substrates with higher conformability to curved surfaces and mechanical flexibility, are required. With the employment of multiple paper-based electrodes located on chest and wrist, heart rate, and respiratory activity are evaluated (see Figure 3e–g). To obtain a reliable analysis and enable proper performance comparison, commercial electrocardiogram (ECG) electrodes are positioned in close proximity to the paper-based ones (see Figure S9, Supporting Information). The electrodes response is measured using a commercial ECG setup (see Experimental Section – Electrical Characterization). To demonstrate the quality of the acquisition setup, data consistency is shown among different body zones (wrist and chest) and electrode types (standard vs paper-based). Although signal

© 2023 The Authors. Advanced Functional Materials published by Wiley-VCH GmbH

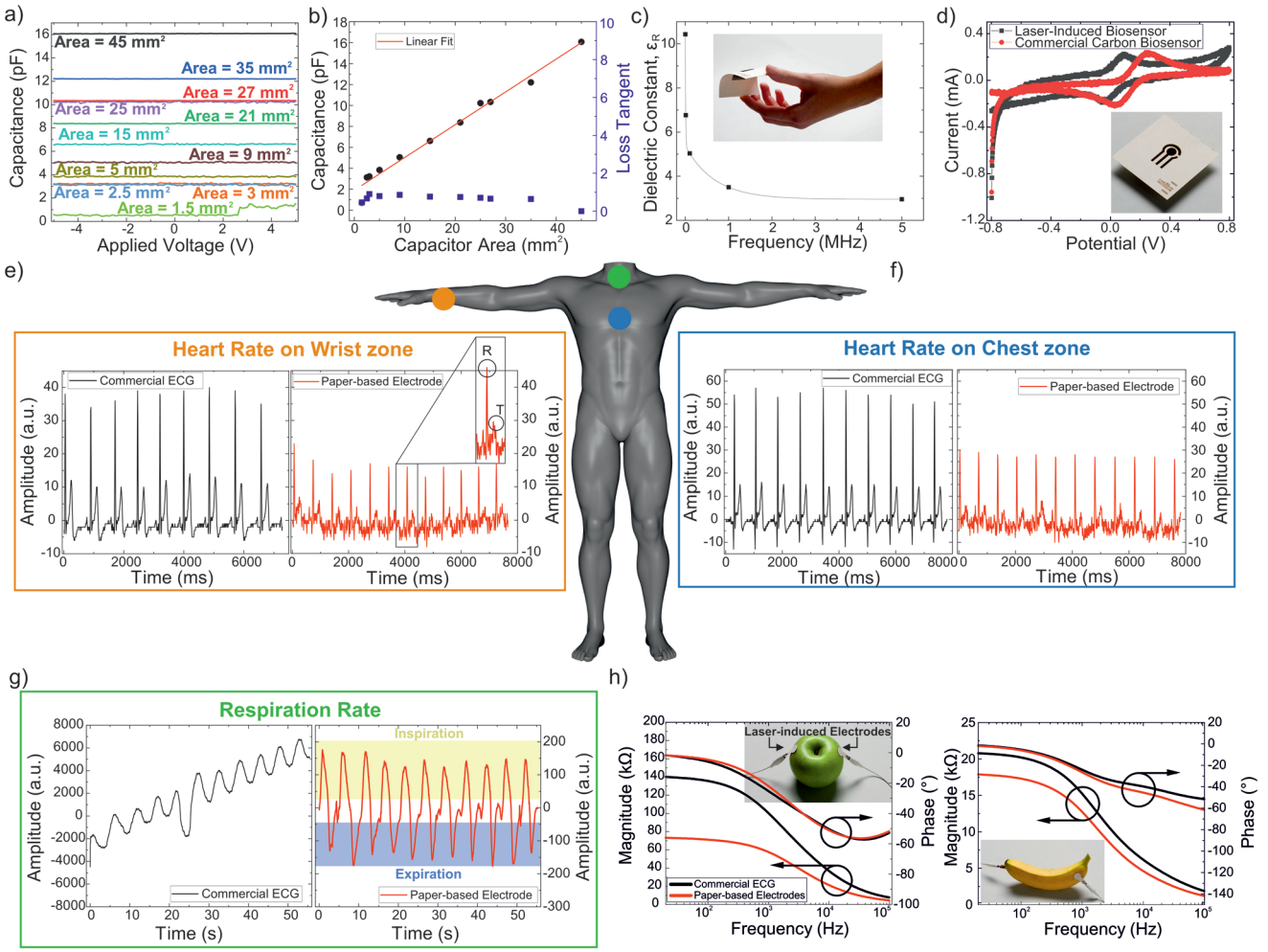

Figure 3. Laser-induced electronics on apple-based paper. a–c) Electrical characterization of parallel plate capacitors, realized by carbonizing both side of the cellulose. b) Tunable capacitances and loss tangent are reported as function of the parallel plate area at 1 kHz and c) the substrate dielectric constant ε_R as function of frequency (ε_R of 2.9 for frequency equal to 5 MHz). d) Characterization of carbonized biosensors and commercial ones. e–g) Comparison between commercial and laser-induced electrodes for on-skin data acquisition applications. Heart activity acquired on e) wrist and f) chest zones. g) Respiratory monitoring during rest. h) Impedance spectroscopy (magnitude and phase) of food samples, comparing paper-based electrodes with commercial ECG ones, for apple (left) and banana (right).

amplitude is lower with paper-based electrodes in comparison to commercial ECG, heart rhythm, and R and T waves are visible using laser-induced electrodes (Figure 3e,f). The weak signals associated to P, Q, and S waves are justified by the selection of peripheral lead I, in which the positive and negative electrodes acquiring the ECG signal, are located on the left and right part of the upper body, following the Einthoven's triangle (see Figure S9, Supporting Information).[64,65] In particular, wrist measurements (Figure 3e) are performed by placing the two electrodes on both wrists, and keeping the neutral one on the left ankle (see Figure S9, Supporting Information); whereas, for chest measurements (Figure 3f), the two electrodes are located on the left and right side of the chest, with the neutral one placed on the left hip (see Figure S9, Supporting Information). For these measurements, the electrode positioning is also a key aspect. Indeed, signals with higher amplitude are observed on the chest in comparison to the wrist measurements, due to the shorter distance to the heart. Moreover, thanks to the rough surface of the carbonized electrodes in combination with the human sweat acting as natural electrolyte, no conductive gel is required during data acquisition. To verify device performance in both dry and moist contact with human skin, impedance analysis (magnitude and phase) of an ECG electrode is performed at low (relative humidity < 45%), moderate (45% < relative humidity < 55%) and high (55% < relative humidity < 80%) humidity level, keeping constant temperature (T = 24 °C; see Figure S9, Supporting Information). Apart for dry conditions (relative humidity < 45%) where a magnitude increase of 25% is measured in comparison to room condition (7.8 kΩ at RH = 40%), low variability is evaluated for humidity level above 45% (magnitudes ranging from 5.9 to 6.8 kΩ, and phases from 0° to 1.3°), supporting the application of paper-based electrodes even for real application scenarios.

Along with heart rate, respiration is another important vital sign to constantly monitor. With the setup in Figure S9 (Supporting Information), impedance pneumography,[66,67]

© 2023 The Authors. Advanced Functional Materials published by Wiley-VCH GmbH

16163028, 0, Downloaded from https://onlinelibrary.wiley.com/doi/10.1002/adfm.202210422 by University Of Padova Center Di, Wiley Online Library on [21/02/2023]. See the Terms and Conditions (https://onlinelibrary.wiley.com/terms-and-conditions) on Wiley Online Library for rules of use; OA articles are governed by the applicable Creative Commons License

consisting in the evaluation of chest impedance variation, is used as tracking method for respiration rate (see Figure 3g). As expected, the impedance amplitude rises during inspiration, due to a variation of the dielectric properties of the lungs caused by air filling, and vice versa.[68,69] Given the measurements accuracy, the employed acquisition setup and flexible paper-based electrodes constitute a versatile, low-cost, and simple alternative for monitoring human vital signs.

The electrical stability on curved substrates (e.g., breast, wrist), the absence of any plastics, as well as low fabrication cost, also make our electrodes suitable for food quality monitoring. The evaluation of ripening, spoilage, and maturity stage represents key aspects to fulfill the market requirements and consumers' need.[70] Among the different methods, electrical impedance spectroscopy (EIS)[71] consists in the correlation of the electrical response of a sample as a function of frequency. Using this method, the electrical impedance of several fruits has been studied,[72,73] resulting in useful information on the chemical and structural composition of the fruits. To provide a reliable alternative to commercial ECG electrodes, paper-based electrodes are tested on apple and banana (see Figure 3h). Considering a large-volume consumption of such devices in food industry, the aim is to demonstrate an alternative solution, with similar electrical functionality, and reduced carbon footprint and environmental impact. For direct comparison, impedance measurements are collected from 20 to 100 kHz using both apple-based and commercial electrodes. This frequency range is widely chosen for biological sample analysis using EIS.[70] In contrast to the on-skin applications in Figure 3e–g, where sweat acted as electrolyte, here conductive gel is used to improve the electrical contact between the laser-induced devices and the fruit skin. Although the mechanical conditions during the experiment (bending radius for apple ≈4 cm, and for banana ≈2 cm), our paper electrodes show good correlation with the impedance response previously reported for apples and bananas.[74–77] For both fruits, the magnitude difference at low frequencies between the commercial and paper types electrodes is mainly due to the following reasons: 1) at the fruit-electrode interface, while the highly porous nature of the banana skin (skin roughness ranging from 2.5 µm in unripe cases, to 6.6 µm for ripe ones[78]) provides a good electrode adhesion, the smoother apple skin (roughness ≈1.43 µm[79]) has an opposite effect, rendering the adhesion, and thus the electrical contact, less stable; 2) on the other electrode end, the non-uniformity of the laser-induced carbon is responsible for a non-ideal interface with crocodile clips and wires; 3) wetting effect, due to the use of conductive gel, making the system calibration unreliable over time.

2.3. Chemical Degradation and Biocompatibility

To accomplish a fully sustainable technology, it is crucial to clearly assess how to reuse or dispose the electronics after its lifetime. One approach is represented by chemical dissolution of the devices in solutions, leaving no harmful wastes.[5,80] The aim for transient electronics is to achieve material decomposition in natural and not aggressive solutions, proving a zero-waste technological platform. As consequence of the use of natural paper as substrate, and the employment of laser induction for the realization of carbon-based electronic devices, dissolution tests are performed (see **Figure 4**a) in citric acid, widely known for its usage in cosmetics, food, and pharmacology. For this purpose, a natural solution resembling lemon juice (citric acid concentration 48 g L^{-1}[81]) at room temperature (pH 1.7) and two paper samples (1 cm × 1 cm and 1 cm × 1.5 cm) are utilized. The goal is to prove device solubility in a low-cost, easily accessible, natural, and disposable medium. Electrical resistance of the carbonized electrodes is monitored during the whole period, to evaluate device stability. Apart for a single point (day 20), in which high resistance (≈150 kΩ) is measured due to the partial contact points damaging, the normalized resistance shows stable trend for 27 days (see Figure 4b). At day 28, cellulose samples break apart, making it impossible for any further electrical characterization. Finally, complete dissolution of both cellulose and carbon fibers is achieved within 40 days (see Figure 4a), resulting in an etching rate of 7.3 µm d^{-1}. Degradation tests with higher citric acid concentration (citric acid 1:4 water) and process temperatures (90 °C) are also performed, to prove the tunability of the whole process (see Figure S10, Supporting Information) and to reduce dissolution time (solution pH 1.3). The tuning of the degradation experiments, from low-waste footprint, natural, and room-temperature etchant solution and moderate energy consumption (Figure 4), to fast dissolution and high etching rate (Figure S10, Supporting Information), allows process flexibility and adaptability to any applications, according to the specific requirements (see Figure S10b, Supporting Information). Additional studies will be devoted to the dissolution in neutral solutions (pH ≈7), to verify transient behavior in physiological compounds. Considering a lifetime in this order of magnitude (40 days), our paper-based devices can provide stable functionality for different applications, such as on-field agriculture and food monitoring.

To evaluate the technology feasibility for on-skin and human-centered applications, it is crucial to study the biocompatibility of our carbonized devices. To fulfil this requirement, human dermal fibroblasts (HDFs) are chosen as appropriate cell line to test cytotoxicity and tolerance on skin.[82] Thus, HDFs are seeded and grown on three sample types, consisting in virgin apple-based paper, FR-treated paper, and carbonized paper with FR treatment (see Figure S11a, Supporting Information) and cell adhesion and proliferation is monitored. This analysis is carried out for 14 days by live/dead assay, and it is run in parallel with cells seeded and grown in polystyrene dishes, used as positive control (CTRL+) (see Experimental Section – Cell Culture, Adhesion, Viability, and Proliferation). Cell adhesion is analyzed after 24 h (time T0) from seeding, whereas cell viability and proliferation is evaluated after 3 days (time T1) and after 14 days (time T2; see Figure S11b, Supporting Information). Red (dead cells)- Green (live cells) fluorescence cell viability assay contains BOBO-3 Iodide (emission 602 nm) as dead cell indicator, and calcein, AM, cell permeant dye (emission 515 nm) as live cell indicator. Few live cells (green emission) are visible in confocal fluorescence images on all the sample types at both T1 and T2, confirming the adequate biocompatibility of the skin-electrode substrate (see Figure 4c). At the end of the experiment (T2), all the polystyrene dishes are investigated under optical microscope. As shown in Figure S11c (Supporting Information), cell colonies are observable for the

© 2023 The Authors. Advanced Functional Materials published by Wiley-VCH GmbH

16163028, 0, Downloaded from https://onlinelibrary.wiley.com/doi/10.1002/adfm.202210422 by University Of Padova Center Di, Wiley Online Library on [21/02/2023]. See the Terms and Conditions (https://onlinelibrary.wiley.com/terms-and-conditions) on Wiley Online Library for rules of use; OA articles are governed by the applicable Creative Commons License

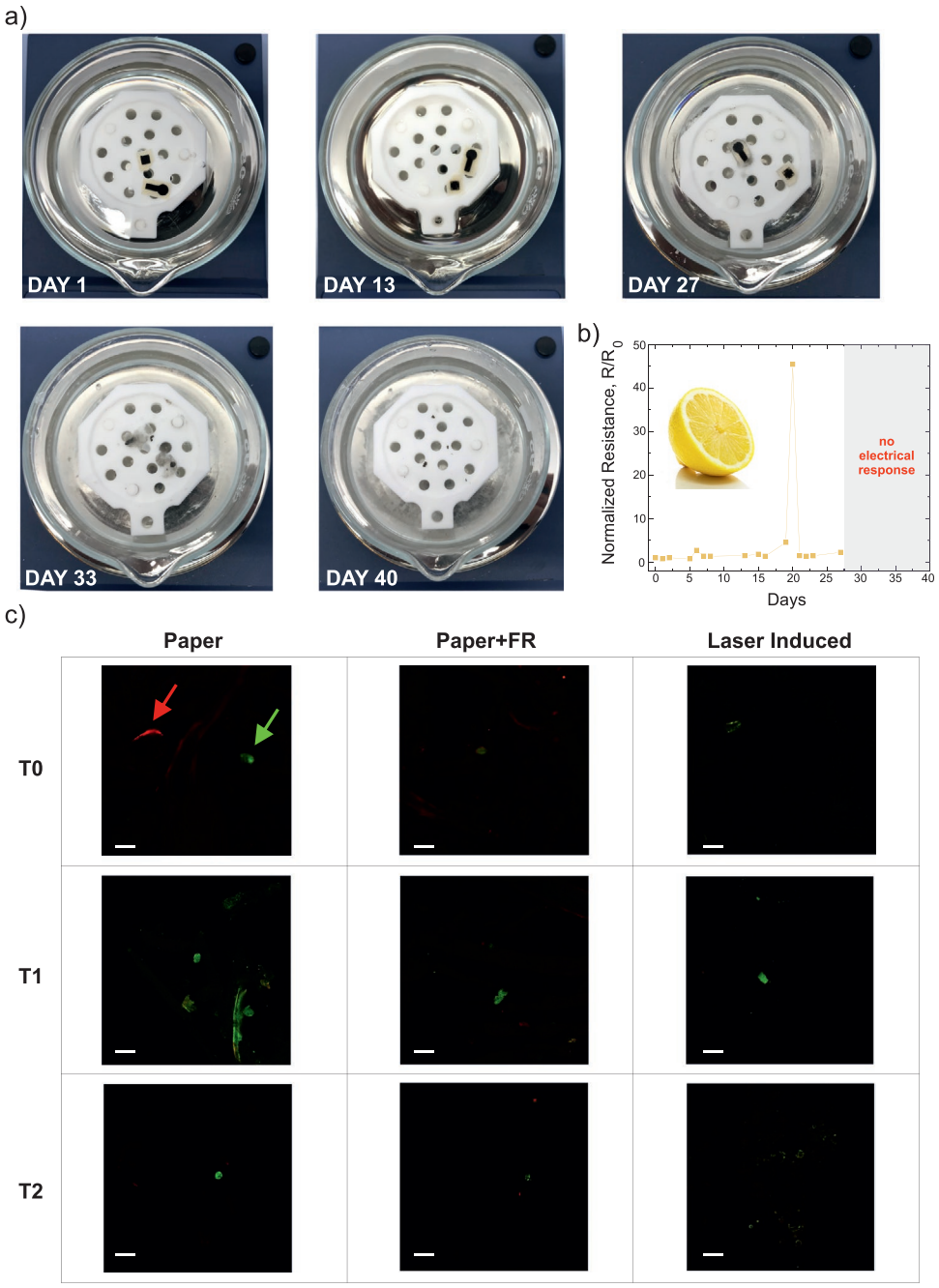

Figure 4. Transient behavior and biocompatibility. a) Paper-based capacitors and electrodes dissolution in lemon juice solution during 40 days. b) Monitoring of the electrical resistance during the dissolution period up to the dissolution of the carbonized layer on day 27. c) Confocal fluorescence microscope images of HDFs seeded and grown on the three paper types at different experiment times (T0 after 24 h from seeding, T1 after three days and T2 after fourteen days) using live/dead assay (Scale bar: 30 µm). Red and green arrowheads indicate dead (red emission) and live (green emission) cells, respectively.

three polystyrene dishes where the different paper samples are immersed and for the CTRL+. This proves that human fibroblasts growth is more desirable on plastic dishes, rather than on paper surfaces. At the same time, the presence of paper samples and the laser-induced materials, as well as the use of FR-treated paper in the growth medium for almost 2 weeks reveal no cyto-toxicity or incompatibility with cell growth, making this technology suitable for biomedical and on-skin applications. The impact of the growth medium on the electrical response of the sample is also evaluated by monitoring the conductivity change during the course of the experiment (see Figure S11d, Supporting Information). After an initial increase in the first days (up to day 6), the electrical resistance stabilizes over time, proving reliable functionality after 14 days immersion time.

© 2023 The Authors. Advanced Functional Materials published by Wiley-VCH GmbH

16163028, 0, Downloaded from https://onlinelibrary.wiley.com/doi/10.1002/adfm.202210422 by University Of Padova Center Di, Wiley Online Library on [21/02/2023]. See the Terms and Conditions (https://onlinelibrary.wiley.com/terms-and-conditions) on Wiley Online Library for rules of use; OA articles are governed by the applicable Creative Commons License

2.4. Circular and Fully Sustainable Electronics

A key aspect for a green technology is the reintroduction of the electronics in nature, through repairing or recycling methodologies.[83] Since our electronics are implemented on plant-derived natural substrate and realized with no harmful materials, it can find application in agriculture. To verify whether our devices can be employed in the soil having no toxic effects on natural ecosystems, elemental analysis is performed on virgin apple-based paper, paper with FR and carbonized paper (see Experimental Section – Elemental Analysis on Paper). This analysis is used to reveal presence of macro- and micronutrients, such as phosphorus (P), potassium (K), iron (Fe), and calcium (Ca),[84] as well as prevent any toxicants. Encouraged by positive response of the different paper types (see Figure S12, Supporting Information), further experiments are performed. To verify the possibility to reintroduce the paper-based electronics into ecosystems, we performed a series of toxicity analysis through seed germination tests directly on the papers (see Experimental Section – Germinations Tests).[85] Here, tomato (*Solanum lycopersicum* L.) is used as a plant species due to its sensitivity toward environmental stresses.[86] Although no inorganic toxic elements are identified in the FR, no seed has germinated on the paper with this solution, indicating the presence of substances inhibiting germination. This might indicate that the toxic substance is of organic nature. On the contrary, seeds have germinated on control paper (acting as reference), virgin paper (see Figure S13, Supporting Information) and carbonized paper without FR (see **Figure 5**a). This fact strongly supports that the flame retardant is responsible for hindering the germination. Therefore, a change to a more biocompatible flame retardant would most likely enable plant growth and thus enabling to discard the whole sensor system in the environment. Comparing the control with both virgin and carbonized papers, no statistical differences regarding the germination number and the Relative Germination Index (RGI) (see Experimental Section – Germinations Tests) are revealed (see Figure 5b). Root weight is significantly higher (+56%) in seedlings germinated on the control sample compared to the carbonized paper, while the normal cellulose exhibited intermediate values. A similar trend is observed for the shoot weight, with the control treatment showing the significantly highest value (+47% with respect to the apple-based paper). Furthermore, control seedlings revealed the significantly longest shoots, being on average 33% higher than the ones germinated on the other two paper types (see Figure 5b). This may indicate that the elements on the carbonized paper are not in a bioavailable form or that growth-inhibiting organic substances

a)

b)

Parameter	CTRL	Apple paper	Carbonized Paper	p-value
# germinated seed	8.29 ± 1.25	7.85 ± 1.67	8.71 ± 0.75	ns*
Relative Germination Index (RGI)	-	94.5%	105.1%	-
Root weight (mg)	4.06 ± 0.99a	3.01 ± 0.95ab	2.6 ± 0.35b	0.011*
Shoot weight (mg)	3.86 ± 1.08a	2.63 ± 0.91b	2.92 ± 0.48ab	0.039*
Root-to-Shoot ratio	1.09 ± 0.34	1.26 ± 0.56	0.89 ± 0.09	ns□
Root length (cm)	1.84 ± 0.27	1.54 ± 0.19	1.58 ± 0.18	ns*
Shoot length (cm)	0.91 ± 0.11a	0.71 ± 0.16b	0.66 ± 0.12b	0.008*

c)

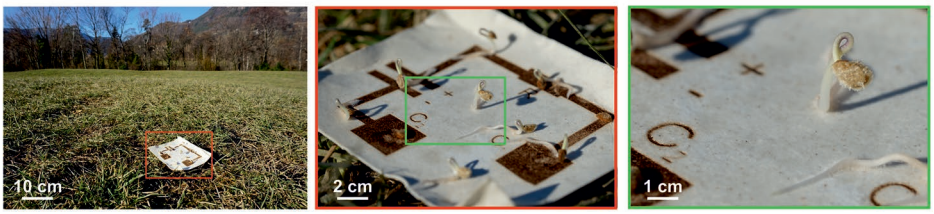

Figure 5. Germination experiments and circular electronics. a) Tomato seeds growth is achieved on large-scale laser-induced papers (Scale bar: 2 cm). b) Comparison of the germination process on different papers: control (CTRL), apple-based and carbonized. c) End of life cycle concept: the electronics can be employed for plant germination, proving a fully sustainable and circular technology.

© 2023 The Authors. Advanced Functional Materials published by Wiley-VCH GmbH

16163028, 0, Downloaded from https://onlinelibrary.wiley.com/doi/10.1002/adfm.202210422 by University Of Padova Center Di, Wiley Online Library on [21/02/2023]. See the Terms and Conditions (https://onlinelibrary.wiley.com/terms-and-conditions) on Wiley Online Library for rules of use; OA articles are governed by the applicable Creative Commons License

developed during the carbonization process. Although the carbonized paper without flame retardant is most likely not usable as fertilizer without additional treatments, it could still be recycled for nonagricultural usage. For sake of clarity, these germination tests are conducted for a short time (72 h) and longer growing periods could potentially eliminate or enforce the encountered down sides. In particular, future works will be focused on additional treatments, employing microorganisms (such as bacteria and fungi[87,88]), to degrade and minimize any organic compounds in the paper with FR. This will further expand the applicability of the presented technology. In addition, this does not detract the possibility to recycle these paper-based electronics as normal paper, considering the absence of any toxic compound (see Figure S12, Supporting Information), and supporting the establishment of a fully circular technology. Although additional experiments will be required to comprehensively understand how the electronics decomposition would take place by microorganisms, these germination tests reveal for the first time the full potential of recycling and reintroduction of electronics in nature (see Figure 5c).

Recent outcomes of the laser-scribing technology are presented in Table S2 (Supporting Information). Although a broad variety of substrates is reported, this technique is widely employed on plastic foils (PET and Polyimide). According to the employed substrate, its nature (natural, synthetic, etc.), as well as its properties (thickness, chemical, and thermal stability), the lasing properties (speed, power, defocus, and use of flame retardant solution) requires performance optimization, to guarantee proper carbonization and reliable electronics performances (see Table S2, Supporting Information) and achieve a technology with high repeatability. Additional effort will be also required on the investigation of natural flame retardant solution, derived from green resources, and easily accessible, since the most widely employed are commercial products, based on sodium borate[38] and phosphate.[36,89] Here, cyto-toxicity tests (see Figure 4c) as well as elemental analysis (Figure S12, Supporting Information) have proved feasibility for on-skin applications and the absence of any toxic compound. In terms of novelty, although supercapacitors have been presented,[27,37,42] a comprehensive analysis of laser-induced capacitors (impedance spectrum, frequency dependence, loss tangent, and dielectric constant analysis), has not been reported yet.[89] For biosensor implementation, the reported performance in Figure 3d (maximum peak current equal to 226 µA) outperforms the state-of-the-art of laser-induced devices realized on PI foils, proving the suitability of the presented approach for disposable and sustainable diagnostics. To reliably investigate full recycling for such devices, additional layers (i.e., sensing membranes, electrolytes, etc.) will be integrated and their impact on the device biocompatibility will be analyzed. For the use of laser-induced electrodes in real application scenarios, the possibility to use the presented devices for respiration activity monitoring, in parallel to fruit quality assessment, is presented here for the first time and it represents a novelty for the establishment of a green and low-cost technology, to be employed in our daily routine with no environmental impact. Moving toward green and low-cost materials, some works have reported the use of paper as carrier (office paper, chromatography paper, phenolic paper).[39,90] Nevertheless, the limited device range and the potential of this plant-derived natural material not fully exploited (i.e., reusability, recyclability, natural dissolution, zero-waste formation), in combination with the result presented here, prove the impact paper-based electronics can have on our environment, prospecting a drastic reduction of e-waste and the evolution of new technologies with low-carbon footprints, to achieve fully sustainable and green electronic systems.

3. Conclusion

In summary, a method for the development of a green, low cost, and environmentally friendly technology for fabrication of electronics is presented. By optimizing the lasing process, conductive amorphous carbonization is induced on commercial recycled paper made from fruit by-products. Capacitors in the pF range, as well as disposable electrodes for monitoring heart and respiration activities as well as fruit monitoring, are demonstrated. The employment of natural layer stacks allows these electronics to be successfully biocompatible with human Fibroblast, for application in wearables and on-skin systems. Two methods to fully recycle the devices after usage are also explored. First, natural dissolution is proved in lemon juice at room temperature within 40 days, leaving no harmful residuals and creating no e-waste. Second, laser-induced electronics on paper is used as support for seed germination and plant growing. The combination of plant-derived natural and plastic-free materials, with low-cost and large-area fabrication method, results in the first demonstration of a fully sustainable and circular technology for applications in food market, medical diagnostics, and smart agriculture.

4. Experimental Section

Substrate Preparation and Induced Carbonization: For the substrate preparation, paper samples, with desired dimensions, were cut from an A0 format paper. First, the paper was immerged in 70 mL of flame retardant (FR) solution (BBT Antiflame) at room temperature. Afterward, the substrate was dried at normal condition under fume hood for 1 day and the leftover quantity of solution was evaluated, to monitor the absorption properties of the paper (see Figures S3–S5, Supporting Information). An Epilog Laser (model: Fusion M2) was used to induce the formation of carbonized layer on the different substrate. The system consists of a CO_2 pulsed laser (maximum power equal to 60 W) at 10.6 µm wavelength and it was connected through wire with a laptop. Through the software supplied by Epilog Laser, a scan speed between 0 and 4200 mm s^{-1} can be selected. An image density of 1200 DPI (maximum allowed value) and 50% duty cycle were adopted. The system supports writing on samples up to 81.4 cm x 50.8 cm, corresponding to 0.26 m^2. Prior starting the writing process, the paper substrate was temporarily attached to a carrier substrate using tape. This guarantees a flat surface during the carbonization process and no focus variation during rastering. On apple-based substrate, the optimized lasing process consists in laser speed of 378 mm s^{-1}, power of 3 W, defocus equal 5 mm and immersion time in flame retardant solution of 2.5 h (see Figure S5, Supporting Information).

Material Analysis: The quality of carbonized layers was investigated with a LabRAM ARAMIS, Raman microscope by Horiba Scientific. All spectra were acquired using the following parameters: excitation line of 633 nm, power density of tens of mW mm^{-2}, grating of 1200 lines mm^{-1}. Each spectrum was obtained with an average of 1 s integration over 50 acquisitions.

© 2023 The Authors. Advanced Functional Materials published by Wiley-VCH GmbH

16163028, 0, Downloaded from https://onlinelibrary.wiley.com/doi/10.1002/adfm.202210422 by University Of Padova Center Di, Wiley Online Library on [21/02/2023]. See the Terms and Conditions (https://onlinelibrary.wiley.com/terms-and-conditions) on Wiley Online Library for rules of use; OA articles are governed by the applicable Creative Commons License

Electrical Characterization: The sheet resistance was evaluated using a four-point probe (Ossila) under ambient conditions. Each sheet resistance value (Figure 2a; Figures S3–S5, Supporting Information) was the average of three measurements collected in three different locations of the test structure. The capacitors were characterized by using an Agilent B1500A parameter analyzer under ambient conditions at different frequencies (1, 10, 100, kHz, 1 and 5 MHz).

For biosensor measurement, reference electrode of the carbonized biosensor was coated with AgCl ink (Loctite EDAG 6038E SS), and cured at room temperature overnight in ambient condition. Commercial carbon biosensors with reference electrode in silver were purchased from Metrohm DropSens (model 110). Three continuous CV measurements were acquired using a VersaSTAT 4 from Ametek Scientific Instruments, with voltage range from +0.8 to –0.8 V, with a scan rate of 125 mV s^{-1}, and using 100 µL of 5 mM $[Fe(CN)_6]^{3-/4-}$ in 0.1 M KCl, as redox mediator, and the third one was reported (see Figure 3d). Among the different measurements, high repeatability was denoted (maximum variation equal to 0.27 mA).

For heart rate and respiratory monitoring, the acquisition setup in Figure S9 (Supporting Information) was used. All human involved in this study were fully volunteered and gave written and informed consent before participation in the study. The study was approved from institutional review approval by the Science and Technology Cross Schools Research Ethics Committee of the University of Sussex (ER/NSM20/2). The electrode triplets (paper-based or commercial) were connected to a ProtoCentral ADS1292R ECG/Respiration breakout kit, interfaced with an Arduino Uno R3 board, to display the real-time measurement. The kit included a differential programmable gain amplifier (PGA), voltage reference, and Analog-to-Digital Converter (ADC). To reduce common mode noise, two electrodes were used as ECG, whereas the third one acts as Driven Right Leg (DRL). Data were collected in series. First, both electrode types were located on the body, following the Einthoven's triangle configuration (see Figure S9, Supporting Information). Then, wire connection to standard ECG was done, to gather the output data. Afterward, similar process was applied on the cellulose-based ones, using crocodile clips. To avoid any sliding on skin and guarantee good adhesion, paper tape was used. No conductive gel was used in this case and all humans were at rest during measurement acquisition. This results in an average sweat level, considering a range of 300–700 mL of sweat perspired by the human body in one day.[91] To evaluate any performance variations of the ECG electrodes and simulate dry or moist contact with skin, a paper-based device was located in a climate chamber (Espec SH-262) and its impedance acquired at room temperature (T = 24°C) with humidity ranging from 35% to 80%, using a bench-top impedance analyzer (Keysight E4990A). Standard connectors were employed to electrically connect the device under test (inside the climate chamber) and the measurement setup (outside the chamber). To verify the environmental condition (temperature and relative humidity) during the experiment, a commercial sensor (SHT4x Smart Gadget from Sensirion) was located in proximity of the device under test (see Figure S9d, Supporting Information). Initially, the device impedance was evaluated at room condition (T = 24 °C and RH = 47%). Next, the impedance measurements were acquired in "dry" condition (RH = 35% and 40%). Afterward, high humidity level (from 50% to 80%) was generated inside the climate chamber and data acquisition was performed.

For the EIS measurements, a Keysight E4990A was employed as impedance analyzer. Prior to start the experiment, the impedance analyzer was calibrated using open, short and a load (resistor of 21 kΩ). Crocodile clips were utilized for proper connection with the electrodes (see Figure 3h). To stabilize the electrode-fruit interface, two electrodes (first, ECG, and later on, paper-based ones) were placed on two opposite points on the fruit skin and left for five minutes before starting any measurement. Here, commercial pre-gelled electrodes, from Kendall ARBO (model: H124SG), were utilized. Magnitude and phase were acquired in a frequency range from 20 Hz to 100 kHz, with logarithmic increment.

To avoid cross contamination due to the presence of external components during the dissolution test (i.e., Cu wires, soldering, etc.), the electrical characterization of the sample was performed on a daily base by taking temporarily the sample out from the beaker and performing the resistance evaluation through the use of a digital multimeter.

Cell Culture, Adhesion, Viability and Proliferation: Human Dermal Fibroblast cells (ThermoFisher, C0135C) were placed at a density of 2.4×10^4 cell mL^{-1} on three different samples, inside four polystyrene dishes. Each dish contains one sample type: one with apple-based papers; one with apple-based papers treated for 2.5 h in FR; one with apple-based papers treated with FR and carbonization process; one left intentionally empty as control (CTRL+; see Figure S11, Supporting Information). Each paper sample was cut in size 2 cm × 2 cm. Cultures were carried out in a growth medium, composed by DMEM (Gibco, 21 969 035) in combination with 15% fetal bovine serum (FBS; Gibco, 10500064), 2 mM L-glutamine (Gibco, A2916801) and 100 UI/ml penicillin–streptomycin (Gibco, 15140148), at 37 °C, 5% CO_2, and humidified incubator. For adhesion analysis, Trypan Blue (Gibco, 15250-061) was mixed in volume ratio 1:1 with Fibroblast cells, which were then counted in a sterilized hemocytometer. After 24 h from cell seeding, the culture medium was replaced in each of the four dishes (T0). This procedure was performed after 3 days (T1) and 14 days (T2) (see Figure S11, Supporting Information). To monitor cell growth, one sample for each type (paper, paper with FR, carbonized paper) was removed from plastic dish and washed in two solutions of PBS (Gibco, 10010015), at each experimental session (T0, T1, and T2). Cells were observed with confocal laser scanning microscopy (CLSM; Leica Microsystems, SP8LIA), equipped with lasers at 488 and 552 nm. For doing this, a live/dead kit (Invitrogen Cell Imaging kit 488/570) was employed to make cell visible under the microscope. Here, red and green colorants were first mixed in a 1:1 ratio, and then drop casted on the paper samples. To raise the protocol efficiency and improve the cell adhesion with colorant solution, papers were incubated for 15 min at 37 °C, 5% CO_2 and humidified environment. To visualize the cell proliferation in the polystyrene dishes at T2 (see Figure S11c, Supporting Information), a Leica DM8000 M optical microscope was used.

Elemental Analysis on Paper: The elemental analysis was performed on the virgin apple-based paper (VP), apple-based paper submersed into the flame retardant (FR) and carbonized paper (CP). Approximately 250 mg of each apple-based paper type was digested with 4 mL concentrated ultrapure HNO_3 (650 mL L^{-1}; Carlo Erba, Milano, Italy) using a single reaction chamber (SRC) microwave digestion system (UltraWAVE, Milestone, Shelton, CT, USA) with 5 mL HNO_3 and 150 mL laboratory grade II water. Following conditions have been used for the mineralization: rise up to 230 °C and 120 bar in 20 min; hold 230 °C and 120 for 10 min. Macro- and micronutrient concentrations were then determined by ICP-OES (SpectroCirosCCD, Spectro, Germany). Experiments were run with three replicates.

Germination Test: Tomato seeds (*Solanum lycopersicum* L. cv Marmande) were soaked in the dark in laboratory grade II water for 24 h. Ten seeds were consequently placed inside 12 cm plastic petri dishes containing a layer of the following paper types: filter paper (Control, CTRL), virgin apple-based paper, paper with FR and, carbonized paper with and without flame retardant. All petri dishes were watered with 3 mL of laboratory grade II water. Petri dishes were sealed with parafilm and incubated at 24 °C in the dark for 72 h. Seven independent biological replicates were used. After 72 h seeds were considered as germinated when the radicle reached 1 mm. Consequently, root/shoot biomass was assessed by weighing. Root/shoot length was measured using Winrhizo software (WinRHIZO Pro2003b, Regent Instruments Inc., Quebec, Canada) with an EPSON1680 high resolution scanner. Relative germination index (RGI, %) was calculated according to the following formula:

$$RGI\,(\%) = \frac{\#\text{ of germinated seeds}}{\#\text{ control germinated seeds}} \times 100 \quad (1)$$

© 2023 The Authors. Advanced Functional Materials published by Wiley-VCH GmbH

16163028, 0, Downloaded from https://onlinelibrary.wiley.com/doi/10.1002/adfm.202210422 by University Of Padova Center Di, Wiley Online Library on [21/02/2023]. See the Terms and Conditions (https://onlinelibrary.wiley.com/terms-and-conditions) on Wiley Online Library for rules of use; OA articles are governed by the applicable Creative Commons License

Supporting Information

Supporting Information is available from the Wiley Online Library or from the author.

Acknowledgements

This study was partially supported by the Free University of Bozen through the Interdisciplinary Call (ID Call 2017, Sustainable Smart Parasites (SSP)) and Research Call (RTD Call Fast 2020, FERMI) and by the Autonomous Province of Bozen-Bolzano/South Tyrol (Provincia Autonoma di Bolzano/Alto Adige – Ripartizione Innovazione, Ricerca, Universitá e Musei) through the International Joint Cooperation between South Tyrol-Switzerland (FLEXIBOTS, grant n.: 2/34). The authors declare no competing financial interest and no conflicts of interest. The authors thank Fabio Valentinuzzi, Christian Ceccon, Andrea La Monica, Elisa Varolo, and Stefano Benini for the support during the biocompatibility test.

Open access funding provided by Universita degli Studi di Modena e Reggio Emilia within the CRUI-CARE agreement.

Conflict of Interest

The authors declare no conflict of interest.

Data Availability Statement

The data that support the findings of this study are available from the corresponding author upon reasonable request.

Keywords

circular and sustainable electronics, flexible electronics, green electronics, healthcare, laser-induced electronics, papers

Received: January 12, 2023
Published online:

[1] The 2030 Agenda for Sustainable Development, **2015**, https://sdgs.un.org/goals.
[2] C. P. Baldé, V. Forti, V. Gray, R. Kuehr, P. Stegmann, *The Global e-Waste Monitor 2017: Quantities, Flows and Resources*, United Nations University, Geneva, Switzerland **2017**.
[3] C. Baldé, V. Forti, V. Gray, R. Kuehr, P. Stegmann, The Global Monitor UNU, Japan **2017**.
[4] D. M. Ceballos, Z. Dong, *Environ. Int.* **2016**, *95*, 157.
[5] K. K. Fu, Z. Wang, J. Dai, M. Carter, L. Hu, *Chem. Mater.* **2016**, *28*, 3527.
[6] W. Li, Q. Liu, Y. Zhang, C. a. Li, Z. He, W. C. Choy, P. J. Low, P. Sonar, A. K. K. Kyaw, *Adv. Mater.* **2020**, *32*, 2001591.
[7] M. Irimia-Vladu, E. D. Głowacki, G. Voss, S. Bauer, N. S. Sariciftci, *Mater. Today* **2012**, *15*, 340.
[8] R. Li, L. Wang, D. Kong, L. Yin, *Bioact. Mater.* **2018**, *3*, 322.
[9] H. Liu, M. Li, C. Ouyang, T. J. Lu, F. Li, F. Xu, *Small* **2018**, *14*, 1801711.
[10] S. Lin, H. Yuk, T. Zhang, G. A. Parada, H. Koo, C. Yu, X. Zhao, *Adv. Mater.* **2016**, *28*, 4497.
[11] G. Cantarella, C. Vogt, R. Hopf, N. Münzenrieder, P. Andrianakis, L. Petti, A. Daus, S. Knobelspies, L. Büthe, G. Tröster, *ACS Appl. Mater. Interfaces* **2017**, *9*, 28750.
[12] P. Lugoda, J. C. Costa, L. A. Garcia-Garcia, A. Pouryazdan, Z. Jocys, F. Spina, J. Salvage, D. Roggen, N. Münzenrieder, *Adv. Mater. Technol.* **2021**, *6*, 2000780.
[13] M. Irimia-Vladu, P. A. Troshin, M. Reisinger, L. Shmygleva, Y. Kanbur, G. Schwabegger, M. Bodea, R. Schwödiauer, A. Mumyatov, J. W. Fergus, *Adv. Funct. Mater.* **2010**, *20*, 4017.
[14] R. Martins, A. Nathan, R. Barros, L. Pereira, P. Barquinha, N. Correia, R. Costa, A. Ahnood, I. Ferreira, E. Fortunato, *Adv. Mater.* **2011**, *23*, 4491.
[15] E. Fortunato, N. Correia, P. Barquinha, L. Pereira, G. Gonçalves, R. Martins, *IEEE Electron Device Lett.* **2008**, *29*, 988.
[16] S. Khan, S. Ali, A. Bermak, *Sensors* **2019**, *19*, 1230.
[17] S. Khan, L. Lorenzelli, R. S. Dahiya, *IEEE Sens. J.* **2014**, *15*, 3164.
[18] M. A. C. Angeli, M. Ciocca, L. Petti, P. Lugli, *Adv. Chem. Eng.* **2021**, *57*, 45.
[19] Y. Chyan, R. Ye, Y. Li, S. P. Singh, C. J. Arnusch, J. M. Tour, *ACS Nano* **2018**, *12*, 2176.
[20] A. F. Carvalho, A. J. Fernandes, C. Leitão, J. Deuermeier, A. C. Marques, R. Martins, E. Fortunato, F. M. Costa, *Adv. Funct. Mater.* **2018**, *28*, 1805271.
[21] A. Kaidarova, M. A. Khan, M. Marengo, L. Swanepoel, A. Przybysz, C. Muller, A. Fahlman, U. Buttner, N. R. Geraldi, R. P. Wilson, *npj Flexible Electron.* **2019**, *3*, 1.
[22] Y. Ling, W. Pang, X. Li, S. Goswami, Z. Xu, D. Stroman, Y. Liu, Q. Fei, Y. Xu, G. Zhao, *Adv. Mater.* **2020**, *32*, 1908475.
[23] X. Chen, F. Luo, M. Yuan, D. Xie, L. Shen, K. Zheng, Z. Wang, X. Li, L. Q. Tao, *Adv. Funct. Mater.* **2019**, *29*, 1904706.
[24] Y. Wang, Y. Wang, P. Zhang, F. Liu, S. Luo, *Small* **2018**, *14*, 1802350.
[25] A. F. Carvalho, A. J. Fernandes, R. Martins, E. Fortunato, F. M. Costa, *Adv. Mater. Technol.* **2020**, *5*, 2000630.
[26] F. J. Romero, I. Ortiz-Gomez, A. Salinas, D. P. Morales, N. Rodriguez, A. Rivadeneyra, presented at IEEE Sensors, IEEE, Texas USA **2020**.
[27] C. Zhang, Y. Xie, C. Zhang, J. Lin, *Carbon* **2019**, *153*, 585.
[28] P. Nayak, N. Kurra, C. Xia, H. N. Alshareef, *Adv. Electron. Mater.* **2016**, *2*, 1600185.
[29] J. An, T.-S. D. Le, Y. Huang, Z. Zhan, Y. Li, L. Zheng, W. Huang, G. Sun, Y.-J. Kim, *ACS Appl. Mater. Interfaces* **2017**, *9*, 44593.
[30] G. Xu, Z. A. Jarjes, V. Desprez, P. A. Kilmartin, J. Travas-Sejdic, *Biosens. Bioelectron.* **2018**, *107*, 184.
[31] D. Konios, C. Petridis, G. Kakavelakis, M. Sygletou, K. Savva, E. Stratakis, E. Kymakis, *Adv. Funct. Mater.* **2015**, *25*, 2213.
[32] J. Kim, J.-H. Jeon, H.-J. Kim, H. Lim, I.-K. Oh, *ACS Nano* **2014**, *8*, 2986.
[33] T.-Y. Zhang, Q. Wang, N.-Q. Deng, H.-M. Zhao, D.-Y. Wang, Z. Yang, Y. Liu, Y. Yang, T.-L. Ren, *Appl. Phys. Lett.* **2017**, *111*, 121901.
[34] A. Rivadeneyra, J. F. Salmeron, N. Rodriguez, D. P. Morales, R. Colella, F. P. Chietera, L. Catarinucci, presented at *2020 50th European Microwave Conf. (EuMC)*, IEEE, Berlin **2021**.
[35] L. Li, J. Zhang, Z. Peng, Y. Li, C. Gao, Y. Ji, R. Ye, N. D. Kim, Q. Zhong, Y. Yang, *Adv. Mater.* **2016**, *28*, 838.
[36] B. Kulyk, B. F. Silva, A. F. Carvalho, S. Silvestre, A. J. Fernandes, R. Martins, E. Fortunato, F. M. Costa, *ACS Appl. Mater. Interfaces* **2021**, *13*, 10210.
[37] X. Zang, C. Shen, Y. Chu, B. Li, M. Wei, J. Zhong, M. Sanghadasa, L. Lin, *Adv. Mater.* **2018**, *30*, 1800062.
[38] T. Pinheiro, S. Silvestre, J. Coelho, A. C. Marques, R. Martins, M. G. F. Sales, E. Fortunato, *Adv. Mater. Interfaces* **2021**, *8*, 2101502.
[39] Y. Chyan, J. Cohen, W. Wang, C. Zhang, J. M. Tour, *ACS Appl. Nano Mater.* **2019**, *2*, 3007.
[40] L.-Q. Tao, H. Tian, Y. Liu, Z.-Y. Ju, Y. Pang, Y.-Q. Chen, D.-Y. Wang, X.-G. Tian, J.-C. Yan, N.-Q. Deng, *Nat. Commun.* **2017**, *8*, 1.
[41] R. Beams, L. G. Cançado, L. Novotny, *J. Phys.: Condens. Matter* **2015**, *27*, 083002.
[42] R. Ye, Y. Chyan, J. Zhang, Y. Li, X. Han, C. Kittrell, J. M. Tour, *Adv. Mater.* **2017**, *29*, 1702211.

© 2023 The Authors. Advanced Functional Materials published by Wiley-VCH GmbH

16163028, 0, Downloaded from https://onlinelibrary.wiley.com/doi/10.1002/adfm.202210422 by University Of Padova Center Di, Wiley Online Library on [21/02/2023]. See the Terms and Conditions (https://onlinelibrary.wiley.com/terms-and-conditions) on Wiley Online Library for rules of use; OA articles are governed by the applicable Creative Commons License

[43] Z. Zhu, Z. Chen, Q. Zhou, D.-W. Sun, H. Chen, Y. Zhao, W. Zhou, X. Li, H. Pan, *Food Bioprocess Technol.* **2018**, *11*, 1615.
[44] D. Arrieta-Baez, M. d. J. Perea Flores, J. V. Méndez-Méndez, H. F. Mendoza León, M. B. Gómez-Patiño, *Molecules* **2020**, *25*, 5955.
[45] M. Ahmad, G. Cantarella, M. A. C. Angeli, M. Madagalam, C. Ebner, M. Ciocca, R. Riaz, P. Ibba, M. Petrelli, I. Merino, presented at 2021 IEEE Int. Flexible Electronics Technology Conf., IEEE, California **2021**.
[46] J. Markell, E. Baker, I. J. Garrett Gu, C. Lansdowne, R. Thakkar, E. Zhou, R. Zhou, J. Ye, *Science Department, All Saints Episcopal School*, Tyler, TX, USA **2016**.
[47] S. Nandy, S. Goswami, A. Marques, D. Gaspar, P. Grey, I. Cunha, D. Nunes, A. Pimentel, R. Igreja, P. Barquinha, *Adv. Mater. Technol.* **2021**, *6*, 2000994.
[48] H. Tai, Z. Duan, Y. Wang, S. Wang, Y. Jiang, *ACS Appl. Mater. Interfaces* **2020**, *12*, 31037.
[49] N. Verma, A. Bhardwaj, *Appl. Biochem. Biotechnol.* **2015**, *175*, 3093.
[50] B. Shkodra, B. Demelash Abera, G. Cantarella, A. Douaki, E. Avancini, L. Petti, P. Lugli, *Biosensors* **2020**, *10*, 35.
[51] A. Douaki, B. Demelash Abera, G. Cantarella, B. Shkodra, A. Mushtaq, P. Ibba, A. Inam, L. Petti, P. Lugli, *Nanomaterials* **2020**, *10*, 1167.
[52] M. Sireesha, V. Jagadeesh Babu, A. S. Kranthi Kiran, S. Ramakrishna, *Nanocomposites* **2018**, *4*, 36.
[53] N. P. Shetti, A. Mishra, S. Basu, R. J. Mascarenhas, R. R. Kakarla, T. M. Aminabhavi, *ACS Biomater. Sci. Eng.* **2020**, *6*, 1823.
[54] C. Fenzl, P. Nayak, T. Hirsch, O. S. Wolfbeis, H. N. Alshareef, A. J. Baeumner, *ACS Sens.* **2017**, *2*, 616.
[55] A. R. Cardoso, A. C. Marques, L. Santos, A. F. Carvalho, F. M. Costa, R. Martins, M. G. F. Sales, E. Fortunato, *Biosens. Bioelectron.* **2019**, *124*, 167.
[56] A. C. Marques, A. R. Cardoso, R. Martins, M. G. F. Sales, E. Fortunato, *ACS Appl. Nano Mater.* **2020**, *3*, 2795.
[57] P. Joshi, R. Mishra, R. J. Narayan, *Curr. Opin. Biomed. Eng.* **2021**, *18*, 100274.
[58] W. Yang, K. R. Ratinac, S. P. Ringer, P. Thordarson, J. J. Gooding, F. Braet, *Angew. Chem., Int. Ed.* **2010**, *49*, 2114.
[59] W. Li, C. Tan, M. A. Lowe, H. D. Abruna, D. C. Ralph, *ACS Nano* **2011**, *5*, 2264.
[60] W. Yuan, Y. Zhou, Y. Li, C. Li, H. Peng, J. Zhang, Z. Liu, L. Dai, G. Shi, *Sci. Rep.* **2013**, *3*, 1.
[61] J. P. Chambers, B. P. Arulanandam, L. L. Matta, A. Weis, J. J. Valdes, *Curr. Issues Mol. Biol.* **2008**, *10*, 1.
[62] J. Hu, S. Wang, L. Wang, F. Li, B. Pingguan-Murphy, T. J. Lu, F. Xu, *Biosens. Bioelectron.* **2014**, *54*, 585.
[63] Q. Wu, Y. Qiao, R. Guo, S. Naveed, T. Hirtz, X. Li, Y. Fu, Y. Wei, G. Deng, Y. Yang, *ACS Nano* **2020**, *14*, 10104.
[64] G. D. Gargiulo, P. Bifulco, M. Cesarelli, A. L. McEwan, H. Moeinzadeh, A. O'Loughlin, I. M. Shugman, J. C. Tapson, A. Thiagalingam, *Sensors* **2018**, *18*, 2353.
[65] B. Abi-Saleh, B. Omar, *Rev. Cardiovasc. Med.* **2010**, *11*, 33.
[66] P. H. Charlton, T. Bonnici, L. Tarassenko, D. A. Clifton, R. Beale, P. J. Watkinson, J. Alastruey, *Biomed. Signal Process. Control* **2021**, *65*, 102339.
[67] L. M. Posthuma, M. J. Visscher, P. B. Lirk, E. J. van Dijkum, M. W. Hollmann, B. Preckel, *J. Clin. Monit. Comput.* **2020**, *34*, 1285.
[68] P. Nopp, E. Rapp, H. Pfutzner, H. Nakesch, C. Rusham, *Phys. Med. Biol.* **1993**, *38*, 699.
[69] G. Cañadas, C. Dell'Aquila, E. Laciar, presented at *II Latin American Conf. on Bioimpedance*, Springer, Montevideo, Uruguay **2016**.
[70] P. Ibba, A. Falco, B. D. Abera, G. Cantarella, L. Petti, P. Lugli, *Postharvest Biol. Technol.* **2020**, *159*, 110978.
[71] R. F. Muñoz-Huerta, A. d. J. Ortiz-Melendez, R. G. Guevara-Gonzalez, I. Torres-Pacheco, G. Herrera-Ruiz, L. M. Contreras-Medina, J. Prado-Olivarez, R. V. Ocampo-Velazquez, *Sensors* **2014**, *14*, 11492.
[72] A. D. Bauchot, F. R. Harker, W. M. Arnold, *Postharvest Biol. Technol.* **2000**, *18*, 9.
[73] J. R. González-Araiza, M. C. Ortiz-Sánchez, F. M. Vargas-Luna, J. M. Cabrera-Sixto, *Int. J. Food Prop.* **2017**, *20*, 1044.
[74] T. Yovcheva, E. Vozáry, I. Bodurov, A. Viraneva, M. Marudova, G. Exner, *Bulg. Chem. Commun.* **2013**, *45*, 68.
[75] A. Chowdhury, T. Bera, D. Ghoshal, B. Chakraborty, presented at Proc. 2015 Third Int. Conf. on Computer, Communication, Control and Information Technology, IEEE, **2015**.
[76] P. Ibba, M. Crepaldi, G. Cantarella, G. Zini, A. Barcellona, M. Petrelli, B. D. Abera, B. Shkodra, L. Petti, P. Lugli, presented at 2020 IEEE Int. Symp. on Circuits and Systems, IEEE, Auxtin Texas **2020**.
[77] P. Ibba, M. Crepaldi, G. Cantarella, G. Zini, A. Barcellona, M. Rivola, M. Petrelli, L. Petti, P. Lugli, *IEEE Access* **2021**, *9*, 63656.
[78] H. Wang, H. Feng, W. Liang, Y. Luo, V. Malyarchuk, *J. Food Sci.* **2009**, *74*, E8.
[79] T. Ringer, L. Damerow, M. Blanke, *J. Food Sci. Technol.* **2018**, *55*, 4197.
[80] L. Yin, H. Cheng, S. Mao, R. Haasch, Y. Liu, X. Xie, S. W. Hwang, H. Jain, S. K. Kang, Y. Su, *Adv. Funct. Mater.* **2014**, *24*, 645.
[81] K. L. Penniston, S. Y. Nakada, R. P. Holmes, D. G. Assimos, *J. Endourol.* **2008**, *22*, 567.
[82] C. Wiegand, U.-C. Hipler, *Skin Pharmacol. Physiol.* **2009**, *22*, 74.
[83] W. R. Stahel, *Nature* **2016**, *531*, 435.
[84] H. Marschner, *Marschner's Mineral Nutrition of Higher Plants*, Academic Press, Cambridge **2011**.
[85] Y. Luo, J. Liang, G. Zeng, M. Chen, D. Mo, G. Li, D. Zhang, *Waste Manage.* **2018**, *71*, 109.
[86] R. Tiziani, Y. Pii, S. Celletti, S. Cesco, T. Mimmo, *Sci. Rep.* **2020**, *10*, 15970.
[87] D. Ghosal, S. Ghosh, T. K. Dutta, Y. Ahn, *Front. Microbiol.* **2016**, 1369.
[88] S. Mukherjee, B. Sarkar, V. K. Aralappanavar, R. Mukhopadhyay, B. B. Basak, P. Srivastava, O. Marchut-Mikołajczyk, A. Bhatnagar, K. T. Semple, N. Bolan, *Environ. Pollut.* **2022**, 119609.
[89] H. Park, M. Kim, B. G. Kim, Y. H. Kim, *ACS Appl. Nano Mater.* **2020**, *3*, 6899.
[90] L. F. Mendes, A. de Siervo, W. R. de Araujo, T. R. L. C. Paixão, *Carbon* **2020**, *159*, 110.
[91] S. Jadoon, S. Karim, M. R. Akram, A. Kalsoom Khan, M. A. Zia, A. R. Siddiqi, G. Murtaza, *Int. J. Anal. Chem.* **2015**, *2015*.

© 2023 The Authors. Advanced Functional Materials published by Wiley-VCH GmbH

16163028, 0, Downloaded from https://onlinelibrary.wiley.com/doi/10.1002/adfm.202210422 by University Of Padova Center Di, Wiley Online Library on [21/02/2023]. See the Terms and Conditions (https://onlinelibrary.wiley.com/terms-and-conditions) on Wiley Online Library for rules of use; OA articles are governed by the applicable Creative Commons License